

Interaction of Drive Modulation & Cable Parameters on AC Motor Transients

R. Kerkman, *Senior Member, IEEE*, D. Leggate, *Member, IEEE*, G. Skibinski, *Member, IEEE*

Rockwell Automation-Allen Bradley
Standard Drives Business
6400 W. Enterprise Drive P.O. Box 760
Mequon, WI 53092 (414)-242-7151 (414)-242-8300 Fax

Abstract: This paper investigates over-voltage transients on ac induction motors when connected through a cable of arbitrary length to a Variable Frequency Drive (VFD) consisting of a Pulse Width Modulation (PWM) inverter with Insulated Gate Bipolar Transistor (IGBT) power devices. Factors contributing to a motor over-voltage transient equal to a theoretical twice dc bus voltage are first described using existing transmission line analysis. A critical cable distance l_c is defined where this 2 pu over-voltage occurs. However, literature is lacking on how motor voltage transients > 2 pu bus voltage and up to 3 - 4 pu are generated. This phenomenon is observed on *all* PWM inverters with output cable lengths greater than l_c distance. Contributing factors to the > 2 pu over-voltage phenomenon are investigated by exploring the complex interaction between drive modulation techniques, carrier frequency selected, cable natural frequency of oscillation, cable high frequency damping losses and to a lesser extent inverter output rise time. Theoretical calculations of cable frequency and damping are correlated with simulation and experimental results. Novel modifications to the PWM modulator as well as external hardware apparatus are proposed solutions to the > 2 pu over-voltage problem, both are simulated and experimentally confirmed.

I. INTRODUCTION

System efficiency and productivity improvements attainable through Variable Frequency Drives (VFD) have meant an increasing segment of low voltage standard ac induction motors are now operated with Pulse Width Modulation (PWM) voltage source inverters from 0.1 to 800 kW using Insulated Gate Bipolar Transistors (IGBT) as the preferred semiconductor switching device. IGBT switching speed (50 to 400 ns) is an order of magnitude faster than Bipolar Junction Transistors (BJT), so that drive switching efficiency is increased, drive package heat sinks are reduced and higher carrier frequencies (f_c) are possible. Higher f_c improves current wave form quality as well as reducing audible noise in motor laminations.

However, ac motor transient over-voltages resulting from drive-motor-cable dynamic response to inverter pulse voltages have steadily increased in magnitude as semiconductor rise and fall switching times have decreased from Gate Turn-Off (GTO) devices, to BJTs, and presently to IGBTs. This trend has occurred while the peak transient over-voltage ca-

pability of the motor's dielectric insulation system has remained unchanged at ≈ 1200 Vpk [1]. Previously, cable application lengths had to exceed 1000-2000 ft for GTO drives and 500-1000 ft for BJT drives before exceeding motor over-voltage dielectric capability. Presently, IGBT drives may create over-voltages that exceed the safe motor level for cable lengths as low as 50 to 200 ft. Thus, a high percentage of VFD applications are now suspect and provide a motivating factor to characterize how these destructive ac motor transient voltages are generated.

The objective of this paper is to first review factors contributing to motor transient voltages that are < 2 pu (1pu = dc bus voltage). Second, investigate factors contributing to the more complex problem of motor over-voltages > 2 pu bus voltage by using basic physical equations, modeling, simulation and experimental results. Third, propose hardware and software solutions that restrict motor over-voltage to safe operating levels.

II. FACTORS CONTRIBUTING TO MOTOR OVER-VOLTAGE < 2 PU BUS VOLTAGE

Transmission line literature exists that describes transient over-voltages with zero initial charge on cables as shown in Fig. 1. Techniques such as graphical Traveling Wave Analy-

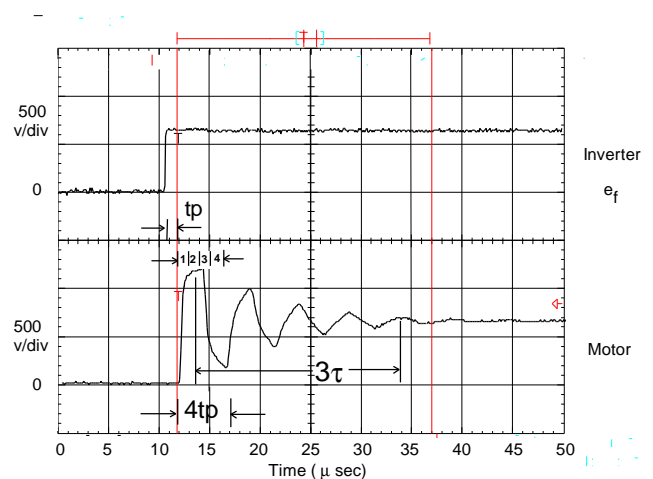


Fig. 1. Experimental results: Transient charging of 500 feet gauge PVC motor cable.

sis [2], Bewley Lattice Diagrams [3], Smith Chart analysis [4], and Standing Wave analysis [1] are available. Factors contributing to motor over-voltage are cable length and cable to motor surge impedance matching, but magnitude and rise time of the PWM output voltage pulses are the predominant factors in this mode as shown in Fig. 2 and explained in [1]. Carrier frequency selection has little effect on motor over-voltage in this mode. Fig. 2 provides a worst case design methodology to estimate motor terminal voltage for an initially uncharged cable condition and assuming complete cable to motor surge impedance mismatch. This allows classical lossless transmission line analysis, treating the motor end as an open circuited line with full voltage reflection taking place. A critical cable distance l_c may be defined where this full theoretical 2 pu over-voltage reflection occurs.

III. FACTORS CONTRIBUTING TO MOTOR OVER-VOLTAGE > 2 PU BUS VOLTAGE

There are certain modes in a PWM modulation cycle that combined with long cable lengths can lead to motor stress greater than the theoretical 2 pu over-voltage with magnitudes of 3 - 4 pu bus voltage possible. Fig. 3 shows such a condition where the last cable transient has not fully decayed before the application of the next pulse so that a residual trapped cable charge condition exists that may lead to 3 pu over-voltage. The effects of these transients > 2 pu are investigated in [5] and shown to have adverse effects on motor dielectric life. A typical pu over-voltage versus cable length curve experimentally derived is shown in Fig. 4 with the l_c distance marked.

In contrast to the conclusions of [6], it is seen that carrier switching frequency and modulation technique have a predominant effect on motor over-voltage in this mode due to the spacing of modulation pulses while inverter rise time has a lesser effect in this mode.

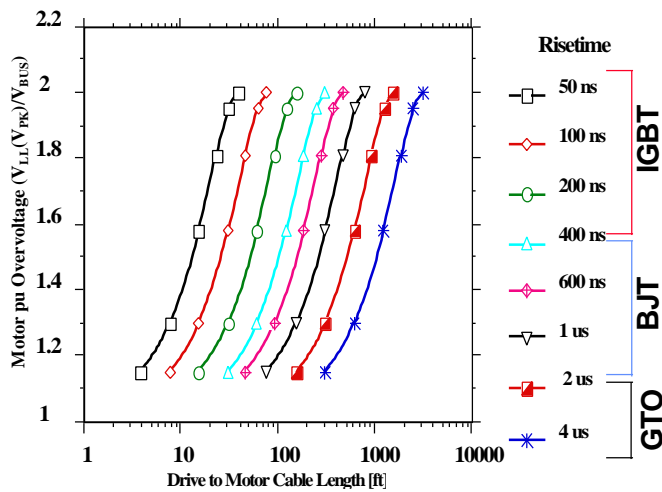


Fig. 2 Motor terminal voltage for uncharged cable.

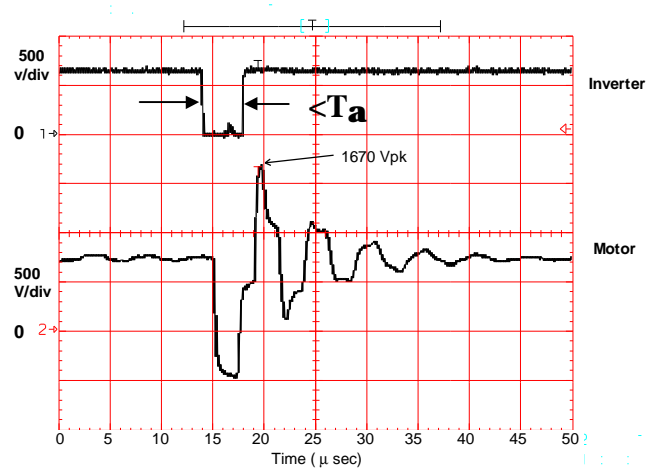


Fig. 3. PWM and the effects of double pulsing.

The cable's natural oscillation frequency has a large influence on cable ac damping resistance which in turn has an effect on how much residual charge is trapped on the cable before the next inverter pulse. A good source on high frequency cable losses has not been found according to [2]. Thus, a technical investigation including the physical equations describing cable oscillation frequency and cable ac high frequency damping resistance is derived and experimentally verified in this section.

A. Oscillation Frequency of Reflected Wave

Fig. 1 shows a single PWM output voltage pulse (e_f) of dc bus magnitude (V_{bus}) traveling down two conductors of a bundled initially uncharged cable. Voltage oscillations around V_{bus} result once the incident wave e_f reaches the motor terminals. Oscillation frequency at the motor terminals is solely determined by cable characteristics and independent of any drive or motor characteristics, including pulse rise time

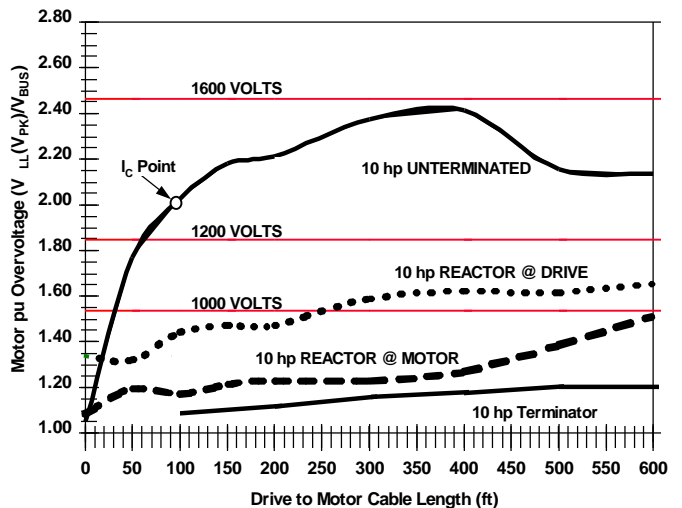


Fig. 4. Terminal voltage experimental data at 480 v.

and hp size. The first oscillation has a theoretical peak of $2V_{bus}$ and a theoretical minimum of zero voltage. Successive oscillations have smaller peak voltage excursions around the V_{bus} pulse level due either to cable resistance damping or reflection coefficient mismatch occurring at both drive and motor ends. Cable oscillation frequency is an important aspect in the creation of > 2 pu motor over-voltage transients and analyzed using 2 conductor transmission line theory. Cable resistance does modify wave velocity slightly. Therefore, lossless line models to estimate oscillation frequency (f_o) are valid.

Inverter output pulse (e_f) travels from drive to motor over cable length distance (a) during cable propagation time (t_p) in Fig. 1. All points in the pulse envelope travel at the same velocity v and pulse shape is propagated without distortion down the line. The \pm sign of (1) indicates that both forward and reverse waves travel at the same velocity. Wave propagation velocity is a function of cable inductance per unit length (L_o) and cable capacitance per unit length (C_o) [1]. Propagation velocity may also be defined using permeability (μ) and permittivity (ϵ) of the dielectric material between conductors [7]. Substitution of free space constants $\mu = \mu_0 \mu_r$ and $\epsilon = \epsilon_0 \epsilon_r$ and setting $\mu_r = 1$ for cable insulations, results in v expressed as a function of relative dielectric constant ϵ_r and speed of light ($c = 3.0 \times 10^8$ m/s) [3]. Velocity v is measured at 1.524×10^8 m/s (50% of c) using $\int x = a = 162$ m (500 ft) and measured t_p of 1μ s from Fig. 1. Velocity v is also estimated at near 50% of c from (1) using typical $\epsilon_r = 4.5$ for a 3 conductor bundled PolyVinylChloride (PVC) insulated wire. Velocity v varies from a low of 32% c for Hypalon ($\epsilon_r \approx 9-11$) bundled wires to 70% c for Teflon ($\epsilon_r = 2.0$) bundled wires. Velocity $v = c$ when widely separated conductors are used, since $\epsilon_r = 1.0$. The following analysis is valid for a typical case where IGBT voltage risetime \leq cable t_p time.

$$v = \frac{\int x}{\int t} = \pm \frac{1}{\sqrt{L_o C_o}} = \frac{1}{\sqrt{\mu \epsilon}} = \frac{c}{\sqrt{\epsilon_r}} \quad (1)$$

The cycle time of the traveling wave relates the cable length to v [7]. To complete one oscillation cycle requires the wave to traverse a four times - $T_{cycle} = 4 t_p$. Thus, f_o may be expressed in terms of cable length and cable characteristics.

Oscillation frequency is inversely proportional to cable length from (2) and graphed in Fig. 5 with the experimental data points for PVC. Thus, high oscillation frequencies occur

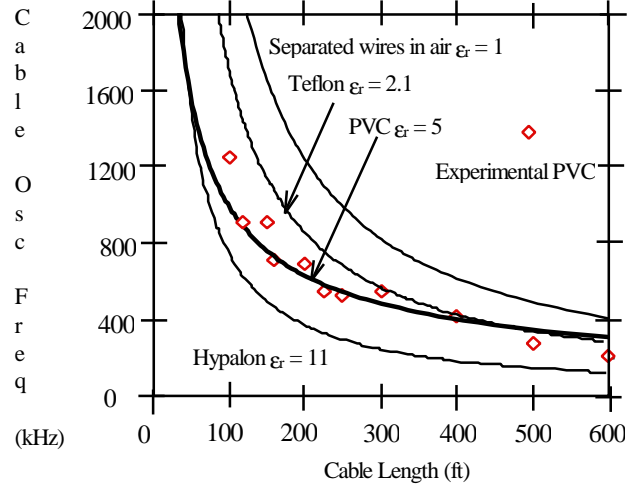


Fig. 5. Oscillation frequency vs cable length.

at short cable lengths. Fig. 5 shows agreement between calculated line and experimental data points. The f_o of Fig. 1 is

$$f_o = 1/T_{cycle} = 1/4t_p = v/4a = 1/4a\sqrt{L_o C_o} \quad (2)$$

250 kHz which agrees with data of Fig. 5. Fig. 5 also shows calculated f_o curves when bundled cables of various insulation types are used.

Cable construction, insulation type and conductor spacing all determine cable parameters L_o and C_o , which define cable wave velocity v . A bundled cable construction compared to widely separated conductors ($\epsilon_r = 1$) results in lower v from (1) and thus a lower f_o from (2). The ϵ_r values of various wire insulation types also affect v , which is directly proportional to f_o from (2).

B. Damping Time of Reflected Waves

Cable oscillation frequency indirectly affects damping characteristics of the over-voltage transient due to conductor ac resistance being increased as a result of skin ($K_{skin}(f_o)$) and proximity (K_p) effects. Resistance losses produce a power loss in the forward PWM voltage pulse e_f , current pulse i_f , and the reflected wave pulses. Heat is dissipated in both the series conductor ac resistance r_s (Ω / unit length) and cable parallel insulation resistance r_p (Ω / unit length), a high ohmic value. The initial pulse amplitude (e_o) will be exponentially attenuated to its final value (e) dependent only on cable constants r_s , Z_o (where $Z_o = \sqrt{L_o/C_o}$), K_p , $K_{skin}(f_o)$, and cable distance x traveled.

$$e/e_o = e^{-(r_s x / 2Z_o)} = e^{-(K_p K_{skin}(f_o) r_{dc} x / 2Z_o)} \quad (3)$$

Thus, tightly bundled phase conductors have greater damping than widely separated conductors, since Z_o of bundled cables is 80 - 150 Ω and is 10 to 20 times lower than for separated conductors [7]. Reflected waves traveling between the drive and the motor dampen quickly since distance ($x = 4a$ in meters) is traveled during each successive oscillation cycle. Also, damping is greater in lower hp drives since smaller gauge wires have higher dc resistance values in the r_s term.

Resistance r_s (ac Ω / conductor / m) is dependent on cable oscillation frequency and is increased above the dc value due to skin and proximity effects. Skin effect is due to the fact that internal inductance of a conductor is highest at the center and least at the edges. Thus, high frequency current oscillating at f_o tends to crowd to the conductor surface, decreasing the apparent conductor area and increasing ac resistance. Proximity effect is due to magnetic fields of a neighboring adjacent conductor distorting and effectively reducing current flow area in the primary conductor. It is sensitive to conductor to conductor spacing. Proximity effect increases ac resistance by a factor of two ($K_p = 2$) in (3) for tightly bundled round conductor cables [8]. The skin effect factor ($K_{skin}(f_o)$) in (3) is a function of frequency [3].

Skin depth of penetration (d) is defined when conductor current density in the radial dimension is at the ε^{-1} value. Substitution of permeability (\mathbf{m}) and conductivity (\mathbf{s}) for copper results in $d_{cu} = 0.0661 / \sqrt{f_o}$ (m) [3]. The total amount of high frequency power carried by the conductor can be described by the Poynting Vector equation ($P_n \propto \varepsilon^{-2} \gamma \delta$) [3]. Substitution of $g = d/2$ yields the radial depth beyond which minimal high frequency power is transmitted. With $g = d_{cu} / 2$, the expression for $K_{skin}(f_o)$ becomes (4) [7].

$$K_{skin(f_o)} = \frac{\mathbf{p} d_o / 4}{\mathbf{p} d} = \frac{d_o}{2 d} = \frac{d_o \sqrt{f_o}}{2(0.0661)} \quad (4)$$

Finally, (5) expresses solid wire copper conductor ac resistance r_s as a function of cable oscillation frequency f_o that includes skin and proximity effects.

$$r_s = K_p K_{skin(f_o)} R_{dc} = K_p \left(\frac{d_o \sqrt{f_o}}{2(0.0661)} \right) \left(\frac{4 \mathbf{r}}{\mathbf{p} d^2} \right) \quad (5)$$

$$= \frac{K_p 16.61 * 10^{-8} \sqrt{f_o}}{d_o}$$

Table I validates predicted r_s values with measured data versus frequency. Prediction of high frequency r_s for large d_o wire is difficult since the number and size of conductor strands is critical.

The time to damp reflected pulses to < 5% of initial peak

TABLE I.
PREDICTED & MEASURED CONDUCTOR AC RESISTANCE VS FREQUENCY.

Wire Gauge		#18		#8	
dc resistance [W/m]		0.01935		0.002132	
do diameter [m]		0.0012446		0.0037338	
ac resistance [Rac/Rdc]		Predicted	Measured	Predicted	Measured
Frequency [kHz]	10	1.4	2.3	4	3.4
	100	4.4	4	13	17
Frequency [MHz]	1	14	14	42	60

value is estimated by substituting $x = \mathbf{n} t$, $v = 1 / (L_o C_o)^{0.5}$ and $Z_o = (L_o / C_o)^{0.5}$ into (3). Reflected wave over-voltages are damped out in a 3τ time interval, with $\tau =$ one time constant $= (2 L_o / r_s)$.

$$\frac{e}{e_o} = e^{-(r_s x / 2 Z_o)} = e^{-(r_s \mathbf{n} t / 2 Z_o)} = e^{-(r_s / 2 L_o) t} = e^{-t / \tau} \quad (6)$$

Fig. 6 graphs calculated 3τ times for bundled cables of various conductor gauges that include skin and proximity effect factors for r_s . A measured skin effect ($L_o \approx 91$ nH / ft at $f_o < 1$ kHz and 85 nH / ft at $f_o > 100$ kHz) was used for all bundled cables [8]. Measured 3τ time from Fig. 1 is ≈ 20 μ s for 500 ft of #12 AWG bundled cable. Calculated f_o oscillation frequency is 250 kHz from Fig. 5, while calculated

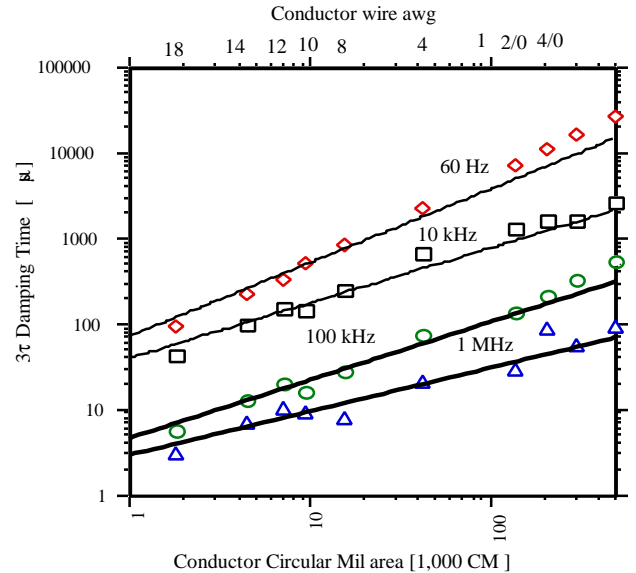


Fig. 6. Calculated 3τ damping time of reflected wave transient for PVC bundled conductor cables.

3τ time from Fig. 6 is $\approx 18 \mu\text{s}$. Measured and calculated 3τ times for wires of #18, #14, and #8 AWG were within 8%.

Fig. 6 shows typical 3τ damping times to reflected wave transients are between the dark solid lines corresponding to cable lengths of 600 ft ($\approx f_o = 200 \text{ kHz}$) and 100 ft ($\approx f_o = 1 \text{ MHz}$). This figure shows skin effect ac resistance has a large influence on damping the reflected transients as compared to the 60 Hz resistance. Fig. 5 also shows the shorter the cable, the higher the f_o and the faster the damping effect from the cable resistance. It is critical to have the reflected wave over-voltage transient oscillation decay to zero before the arrival of the next PWM pulse. For example, the T_{α} time in Fig. 3 is less than 3τ causing the over-voltage transient upon the arrival of the next PWM pulse. Therefore, T_{On} must be greater than $T_a = 3\tau$. This prevents trapped line charge from causing a possible 3 pu over-voltage transient when PWM dwell times (the time when the line-to-line voltage is zero) are short or if carrier frequency is increased, thus reducing allowable decay times.

Low hp ac drives have small cable diameters thus have a reflection coefficient approximately equal to one ($G_m \approx 1$), so that the predominant mechanism of transient over-voltage decay is through skin effect cable resistance damping. High hp ac drives have large cable diameters so over-voltage transient decay from skin effect cable resistance damping in Fig. 6 is minimal. Luckily, these drives have reduced cable to motor G_m coefficients (< 0.9). Thus, the main damping of the reflected waves is obtained by multiplying the reflected wave by these reduced G_m values at each successive f_o cycle until the transient decays. The breakpoint between these two different decay modes is thought to be somewhere in the vicinity of drive hp's using #8 AWG wire.

C. Summary

Existing literature on the effects of long cables emphasize the traditional 2 pu motor terminal voltage. Recent investigations have shown IGBT inverters induce motor over-voltages at 50 ft. This section of the paper has presented experimental data demonstrating > 2 pu motor terminal voltages. The importance of cable natural oscillation frequency (f_o) and its dependency on cable length were presented and experimentally verified. Cable damping time (τ) and its inverse relationship to $\sqrt{f_o}$ was theoretically established and confirmed with experimental results.

IV. THE CONTRIBUTION OF MODULATORS TO MOTOR OVER-VOLTAGE > 2 PU BUS VOLTAGE

Investigations into motor over-voltages caused by IGBT inverters and long cable lengths generally focus on occur-

rences of motor voltages < 2 pu. Although a few investigators have mentioned the possibility of > 2 pu over-voltage, the majority do not explore the contributing factors and consider > 2 pu bus voltage not likely and therefore of little practical significance [4,6,9-15]. Recent motor winding failures precipitated an investigation into the exact nature of the mechanism responsible for motor winding degradation [5]. This investigation discovered motor terminal voltages exceeding 2 times the bus voltage are very probable. Further field experience and laboratory testing confirmed these findings.

A. Motor Voltages in Excess of 2 Times Bus Voltage Caused by Insufficient Dwell Time: The Double Pulsing Effect

1. *Experimental Evidence:* Fig. 3 demonstrates the > 2 pu over-voltage phenomenon. This figure displays the inverter and motor line-to-line voltage for an unloaded 10 hp ac induction motor at 60 Hz. The drive employed a uniform sampled third harmonic PWM (TPWM) modulator and a 4 kHz carrier. A 500 ft #12 gauge cable connected the drive to the motor.

Initially, the cable was in a fully charged condition ($V_i(0) = V_m(0) = V_{\text{bus}}$). A transient disturbance occurs ($V_i(1) = V_i(2) = V_i(3) = 0$) by discharging the cable for approximately $4 \mu\text{s}$ ($<$ dwell time, T_a). The propagation delay between the inverter terminals and motor terminals is fully recognizable and is approximately $1 \mu\text{s}$. As is evident from the data, the reflection coefficient is nearly unity, thus reflecting the incoming negative voltage and forcing the terminal voltage to approximately negative bus voltage ($V_m(1tp) = V_m(0) - V_{\text{bus}}(1 + G_m) \approx -V_{\text{bus}}$). A reflected wave ($-G_m V_{\text{bus}}$) traveling from the motor to the inverter and back requires $2 \mu\text{s}$. Prior to the arrival of the reflected wave, the terminal voltage tracks the characteristic response of the motor cable combination ($V_m(2tp) \approx V_m(1tp)$). With the reflection coefficient of the inverter approximately -1 the reflected wave arrives at the motor terminals ($V_m(3tp) = V_m(2tp) - V_{\text{bus}} G_m (1 + G_m) \gg V_{\text{bus}}$). The reflected wave ($-\Gamma_i \Gamma_m^2 V_{\text{bus}}$) travels from the motor to the inverter where it is reflected and sent back to the motor ($-\Gamma_i^2 \Gamma_m^2 V_{\text{bus}}$). While this is occurring $V_m(4tp) \approx V_m(3tp)$. In addition, at precisely the instant this reflected wave arrives at the motor terminals, the control's pulse ($V_i(4) = V_{\text{bus}}$) arrives. This new pulse is reflected by the motor, with the motor terminal voltage now achieving a peak value of 1670 Vpk ($V_m(5tp) = V_m(4tp) - (\Gamma_i^2 \Gamma_m^2 V_{\text{bus}}) + V_i(4)(1 + G_m) > 2V_{\text{bus}}$ for $G_m < 1$).

The above sequence of events may be referred to as *double pulsing* of a charged motor drive cable system. This contrasts with the single pulsing of charged or uncharged cables as shown in Fig. 1, the voltage of which is limited to 2 times the bus voltage. The amplitude of the double pulsed motor over-voltage, however, is governed by a number of variables.

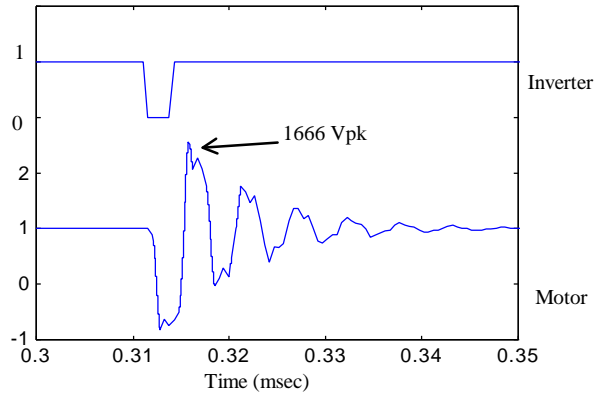


Fig. 7. Simulation of Fig. 3 - 1 pu = 650 v.

Obvious ones include the damping characteristics of the cable, bus voltage, and dwell time of the pulse. Not as obvious, but perhaps more important, are carrier frequency, modulation technique, and duty cycle.

2. *Simulation Results:* Cable parameters were calculated and correlated to typical cables employed in the industry. The parameters were combined with surge impedance values for ac induction motors and simulation studies performed. By varying cable lengths, device rise and fall times, load surge impedance, and control variables including modulation technique, predictions were made of the motor terminal voltage. Fig. 7 shows simulation results for the conditions presented in Fig. 3. The simulation predicts a peak motor voltage of 1666 Vpk with a dominant frequency of approximately 180 kHz and 22 μ s to damp within 5% of bus voltage. This compares favorably with the experimental results, which showed a peak voltage of 1670 Vpk, a frequency of 200 kHz, and 23 μ s.

3. *Effects of Carrier Frequency and Modulator on Motor Over-Voltage:* With the existence of > 2 pu voltage estab-

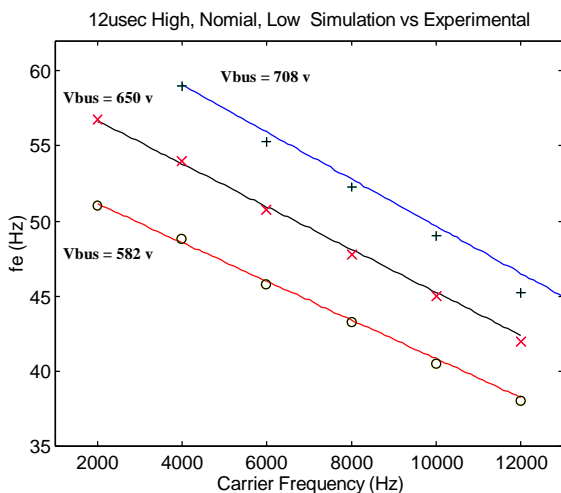


Fig. 8. Double pulsing inception frequency for TPWM.

lished, it is important to understand what contributes to the phenomenon. Clearly damping characteristics of the cable, bus voltage, and dwell time are major contributors. However, double pulsed over-voltages depend on carrier frequency, modulation strategy, and bus voltage [16]. Fig. 8 plots the operating frequency, fe^*a , at which double pulsing begins, as a function of carrier frequency and bus voltage for a TPWM modulator. This frequency, the *double pulsing inception frequency*, also depends on the type of modulation - sine wave, third harmonic, space vector, or two phase [16].

Two items are apparent: First, for a fixed bus voltage, the operating frequency at which inception occurs decreases with increasing carrier frequency. Second, as the bus voltage increases, the inception frequency increases for a fixed carrier frequency. This result, although contrary to those of [12,14], clarifies the contribution of carrier frequency to excessive motor over-voltages. Increasing the carrier frequency increases the occurrences of double pulsing. Increased double pulsing combined with insufficient dwell time, $T\alpha$, provides a scenario for > 2 pu.

B. Motor Over-Voltages Due to Polarity Reversals: A New Contributor to Reflected Waves

Other investigators have discussed the existence of over-voltages > 2 pu induced by double pulsing [13,14]. However, another cause, referred to by the authors as *polarity reversal*, has not received comparable attention. *Polarity reversals* occur when the modulating signals are transitioning into and out of over-modulation or at the point of intersection of the two modulating waveforms.

1. *Experimental Evidence:* Fig. 9 shows the inverter and motor line-to-line voltages for a TPWM ac inverter drive with a 4 kHz carrier and a 10 hp 460 vac induction motor operating at no load and 60 Hz. At bus voltages less than

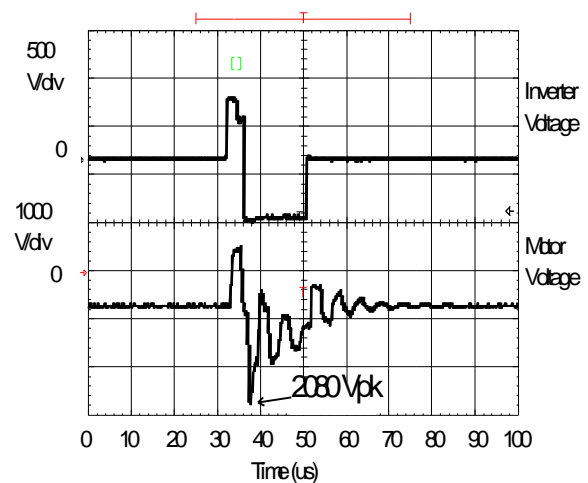


Fig. 9. Effect of polarity reversal.

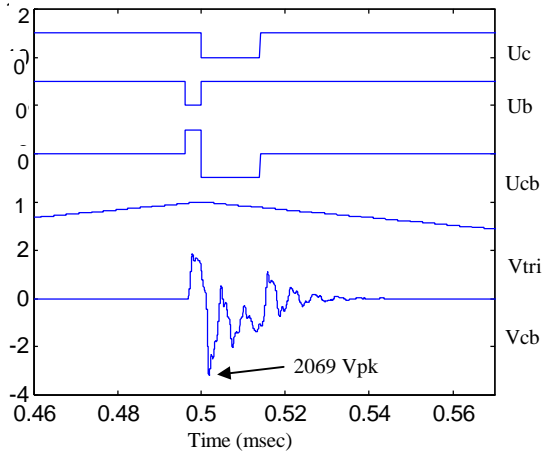


Fig. 10. Simulation of polarity reversal: expanded - $1\text{ pu} = 650\text{ v}$.

640 volts, TPWM's enter into over modulation to maintain rated voltage. For the results of Fig. 9, the bus voltage was reduced to force over-modulation. As the modulating signals transition into and out of over-modulation, the line-to-line inverter voltage generates a *polarity reversal*. The resulting traveling wave excites an extreme voltage transient at the terminals of the machine. The measured voltage exceeded 2000 Vpk or 3 pu. Voltages of this magnitude can cause rapid motor winding failures. Furthermore, at this level even an inverter rated motor's insulation level is exceeded [5].

2. *Simulation Results*: The simulation results displayed in Fig. 10 serve to explain the polarity reversal phenomena and also predict the tremendous over-voltages of Fig. 9. In this figure, two inverter phases U_c and U_b , the line-to-line voltage U_{cb} , the carrier V_{tri} , and the motor line-to-line voltage V_{cb} , are plotted. A 50 ns device rise time was employed in the simulation and is representative of the experimental results of Fig. 9. The line-to-line voltage, U_{cb} , displays the

polarity reversal, the switching of the line-to-line voltage from plus V_{bus} to minus V_{bus} .

As Fig. 10 shows, the predicted peak motor voltage, 2069 Vpk, is in good agreement with the results of Fig. 9. Furthermore, the motor line voltage transient, both oscillation frequency (180 kHz) and 50% damping time (13 μs), compares favorably with the experimental result (200 kHz and 12 μs) of Fig. 9.

V. RESTRICTING MOTOR OVER-VOLTAGES $> 2\text{ PU}$

Many approaches to limiting motor over-voltages $< 2\text{ pu}$ exist [4,6,9-18]. Thus far, these either incorporate passive filters with an attendant increase in drive cost or resort to limiting system parameters, for example IGBT rise time with the penalty of increasing switching losses [1]. This paper presents active and passive solutions to $> 2\text{ pu}$ over-voltage.

The first approach, the *pulse elimination technique (PET)*, modifies the PWM algorithm and prevents *double pulsing* and *polarity reversals*. The second approach, impedance matching technique, terminates the cable at the motor terminals with a passive load that matches the characteristic impedance of the cable. Other solutions, including both software and hardware corrections, may be found in [16].

A. Reducing Motor Over-Voltages: the PET

1. *Analysis*: Fig. 11 shows a per phase block diagram of the PET. To facilitate an understanding of the functioning of the PET, reference is made to the pulse sequences of Fig. 12. The top trace depicts U_c transitioning out of over-modulation. The second trace shows U_b transitioning into over-modulation. The third trace is the line-to-line voltage U_{cb} . Note both a double pulsing and a polarity reversal are depicted. The bottom three traces show the same quantities after processing by the algorithm of Fig. 11.

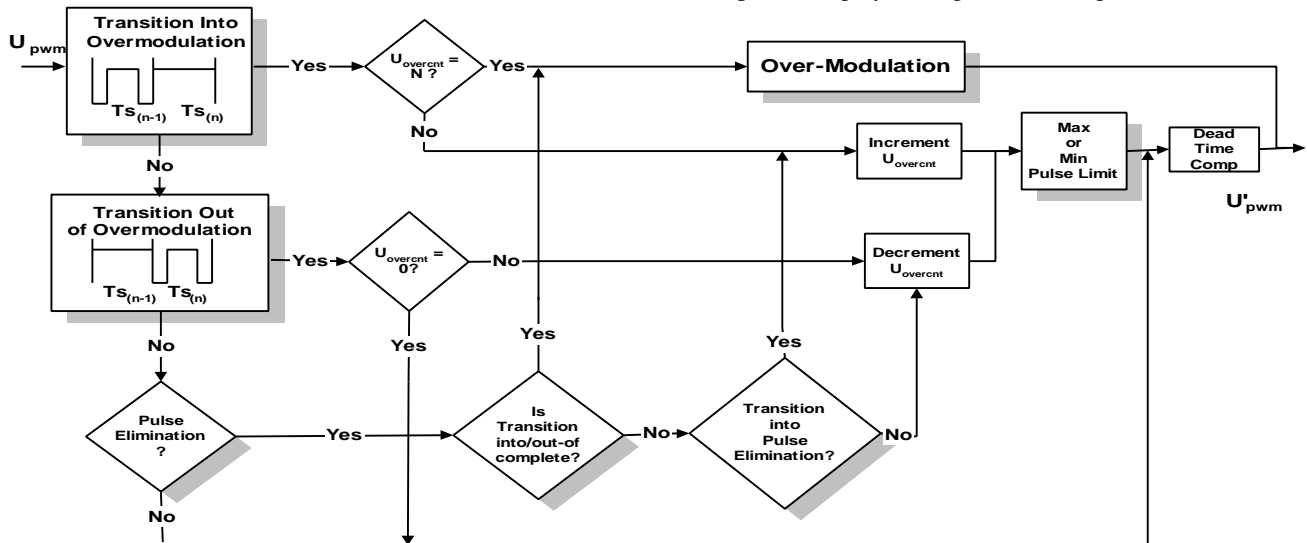


Fig. 11. Per phase block diagram for PET.

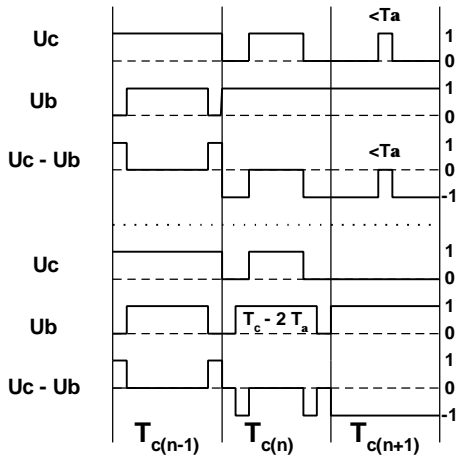


Fig. 12. Processing of pulse sequences by PET.

First, the algorithm determines if a transition into the over-modulation region ($U_{pwm} > T_c$) is occurring. If true, as shown in Fig. 12 for U_b , a counter is checked for a value N , the number of transition cycles. If the counter does not equal N , the counter is incremented and a maximum($T_c - T\alpha$) or minimum($T\alpha$) T_{on} is maintained. This T_{on} is then processed for dead time compensation prior to submittal to a digital comparator. If the counter equals N , then over-modulation is commenced and dead time compensation not implemented.

If a transition exists from the over-modulation region, U_c for example, then the counter is examined for a zero condition. If the counter is nonzero, the counter decrements and a maximum($T_c - T\alpha$) or minimum($T\alpha$) T_{on} is executed prior to processing by the dead time compensation. If the counter is zero, transition from over-modulation is completed and pulse time is processed for dead time compensation. By ensuring the number of decrements equals the number of increments above, the volt seconds are symmetrically placed. The pulse elimination feature compensates for the reduction of the fundamental voltage caused by the volt-second placement.

Finally, if neither of the above conditions are met, the algorithm checks for double pulsing ($T_{on} < T_a$ or $T_{on} > T_c - T_a$). If true and transitioning is complete, the pulse is eliminated and the over-modulation algorithm is executed. In this manner, both *double pulsing* and *polarity reversals* are eliminated, without significantly affecting the fundamental voltage or harmonic content.

2. Experimental Evaluation: The algorithm was implemented in an Intel 80C196MC microprocessor. A TPWM provided the modulation strategy. Experimental evaluations were performed over the operating regions expected of industrial ac drives. Typical results are presented in Fig. 13 with the operating conditions the same as Figs. 3 and 9.

The oscilloscope was triggered on the motor line voltage with the level selected to trap the largest positive and nega-

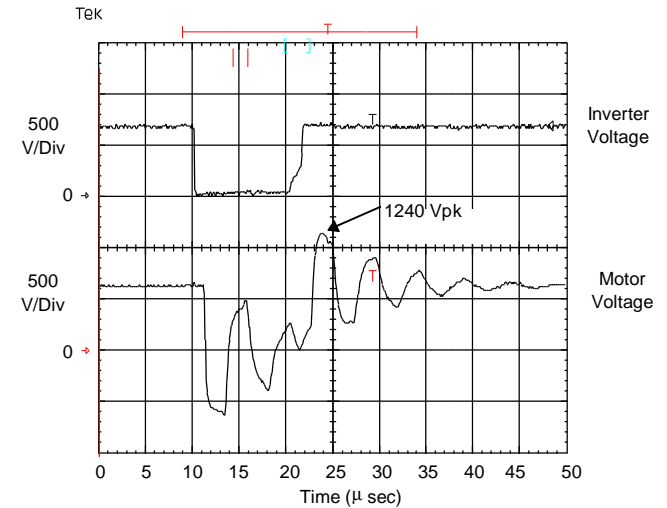


Fig. 13 (a). Fig. 3 with pulse elimination.

tive value. Comparing the results, the *PET* with $T_a = 12 \mu$ s, reduces the peak motor voltage from 1670 Vpk in the *double pulsing* mode of Fig. 3, to 1240 Vpk (Fig. 13a) transitioning into *pulse elimination* of Fig. 12. For polarity reversals, *PET* reduces the maximum voltage from 2080 Vpk (Fig. 9) to 1280 Vpk (Fig. 13b). These reductions, to approximately 2 pu, were accomplished without significantly increasing the sub-carrier harmonic content or the fundamental component of the applied voltage. Fig. 14 shows the per unit motor voltage as a function of cable length for both standard PWM and *PET* PWM. The operating conditions were 60 Hz, no load, 8 kHz carrier, and 650 vdc bus. The improvement provided by *PET* is substantial and maintains terminal voltage within inverter grade motor ratings.

By lowering the motor over-voltage to roughly 2 pu through modifications in the pulse width modulator, other elements incorporated in the system, such as filters, increased device rise time, and inline reactors, now are de-

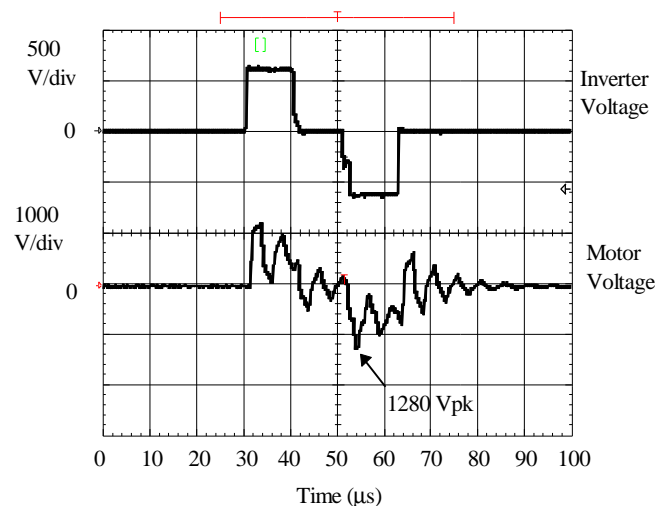


Fig. 13(b). Fig. 5 with polarity reversal correction.

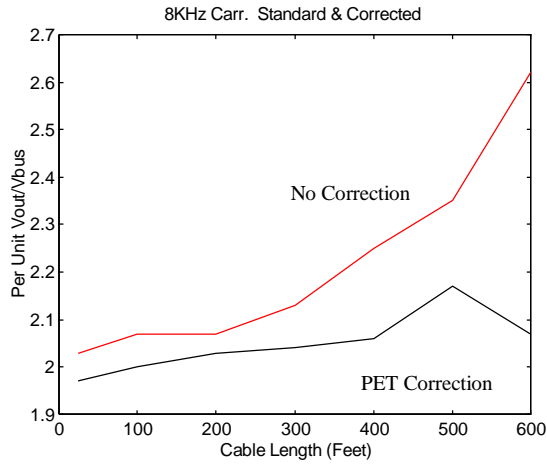


Fig. 14. Per unit data - no correction and PET correction.

signed with a lower voltage objective. This reduces component size for the passive solutions and allows faster power device rise times, thus retaining the benefits of reduced switching losses with high carrier frequencies without adverse motor over-voltages. Furthermore, restricting motor over-voltage to < 1600 Vpk will ensure inverter grade motors need not be derated.

B. Reducing Motor Over-Voltage: Impedance Matching

Passive solutions to the over-voltage problem focus on inserting line reactors or incorporating filters. The line reactors reduce the steep wave fronts presented by the inverter, thereby attenuating the high frequency components of the impressed voltage of Fig. 4. This solution can result in per unit series impedance of up to 3%, with their accompanying fundamental voltage drop; thus, the available motor line voltage and deliverable torque are reduced [14]. Most filter proposals attempt to provide an over damped or critically damped characteristic; however, the filter's performance depends on cable length, making the filter design application dependent, and neglects the effects of *double pulsing* and

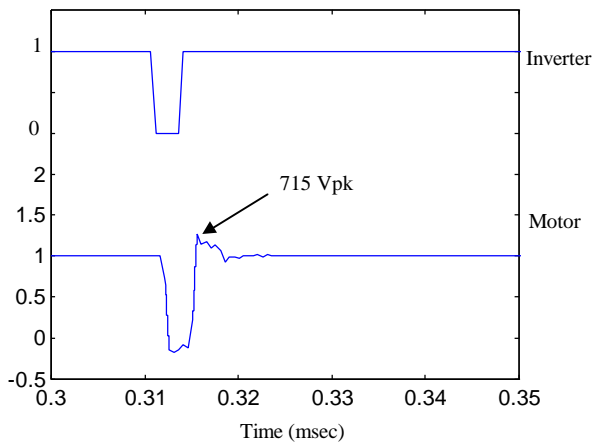


Fig. 15. Simulation of termination impedance.

polarity reversal [10].

Another approach matches the load impedance to the characteristic impedance of the power cables [17-19]. Because the characteristic impedance of a low hp motor is much greater than typical cable characteristic impedance, a termination impedance matched to the cable when placed in parallel at the motor's terminals will provide a load impedance that approximates the cable's characteristic impedance. This will all but eliminate the reflected voltage wave and limit the motor voltage to $\approx V_{bus}$. Unlike a filter, the termination impedance is based on the cable characteristic impedance, and is independent of cable length.

1. *Simulation Results:* Fig. 15 shows the motor's line-to-line voltage in response to an excitation identical to that of Fig. 7. In this case, however, a termination impedance equal to the cable characteristic impedance was added in parallel with the motor. Z_o was $\approx 87 \Omega$ for the cable and $\approx 1000 \Omega$ for the induction motor. Because of the substantial mismatch between cable and motor, the termination impedance dominates and essentially presents a matched load to traveling waves. Notice the peak voltage is now just 715 Vpk, slightly larger than the 650 volt bus.

2. *Experimental Results:* A termination impedance consisting of a line-to-line series combination of resistance and capacitance was designed for #12 gauge cable. The cable's per unit length parameters were: $R_{dc} = 5.4 \cdot 10^{-3} \Omega/m$, $C_o = 106$ pF/m, and $L_o = 780$ nH/m. Incorporating the skin effect factor, the cable's $Z_o \cong 85 \Omega$. For #12 gauge cable, therefore, the termination impedance (R_t and C_t) should approximate the cable's Z_o ; thus, $R_t = 85 \Omega$. The selection of the capacitance is governed by two main factors: limiting the voltage overshoot and ensuring discharge of the capacitance during the dwell time. With the PWM enhancements of *PET*, T_a is known, which allows for an optimization of the termi-

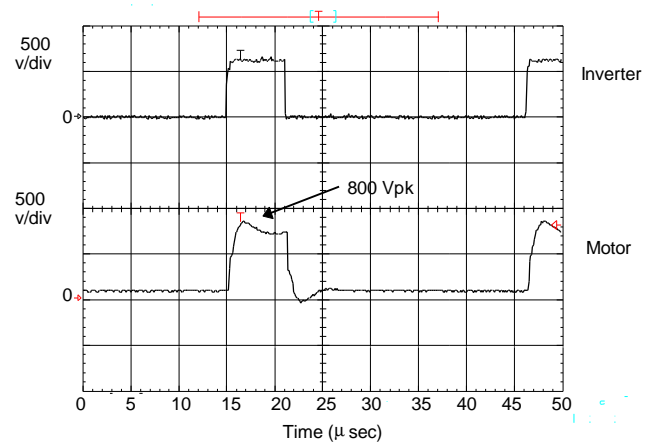


Fig. 16. Motor terminal voltage with termination impedance at 8 kHz.

nation impedance. For the results presented in this paper, $C_t = 0.047 \mu\text{F}$.

Fig. 16 shows the inverter and motor line-to-line voltages with an 8 kHz carrier frequency for the motor drive system of Figs. 3 and 9 with a termination impedance placed at the motor terminals. The results displayed do not incorporate *PET*, thus displaying the improvement obtainable with passive filtering. The peak voltage is now limited to 800 Vpk at 8 kHz.

Fig. 4 includes results for a number of passive solutions. Inserting a series reactor at the inverter reduced the over-voltage by 33%. By moving the reactor to the motor terminals, the over-voltage is reduced by 38%. However, with the termination impedance, the over-voltage is reduced by 50%, maintaining the motor terminal voltage within the guidelines for standard ac induction motors.

Passive corrections, while solutions to motor over-voltages and field retrofitable, have limitations. The losses establish the physical size of the termination impedance and at low hp's result in relatively large and costly systems. Furthermore, the carrier frequency of the drive is limited because of heat dissipation in the termination block. However, experience has shown the termination impedance protects the motor when correctly applied.

VI. CONCLUSION

In this paper, motor over-voltage transients are investigated. The paper reports on two levels of motor over-voltage, < 2 pu and > 2 pu. A critical distance is developed, beyond which motor over-voltages > 2 pu are likely. Contributing factors to < 2 pu voltage, motor-cable impedance mismatch, power device rise time, and cable length, are discussed. The paper presents experimental data showing the tremendous voltages possible with modern IGBT inverters. Factors inducing > 2 pu motor over-voltage are presented, including high frequency cable damping, and PWM pulse patterns. PWM patterns, *double pulsing and polarity reversal*, are identified and correlated to carrier frequency, bus voltage, and modulation strategy. Solutions to motor over-voltages proposed in the paper include the following, which may be implemented independently or in combination: the *pulse elimination technique (PET)*, an active approach, and termination impedance matching, a passive approach.

Major findings reported in the paper are: (1) the importance of *cable natural oscillation frequency* (f_o) in addition to device rise time related excitation frequency in determining maximum motor terminal voltage, (2) *cable damping time* (t) is a significant factor in determining motor over-voltage and is a function of f_o , (3) the discovery of line-to-line voltage *polarity reversal* as a new contributor to motor

over-voltage, (4) PWM carrier frequency influences motor over-voltage through the dwell time in double pulsing, (5) the type of modulator establishes the operating regions where motor over-voltage is of concern.

REFERENCES

- [1] S. Evon, D. Kempke, L. Saunders, and G. Skibinski, "IGBT Drive Technology Demands New Motor and Cable Considerations," Accepted for presentation at the 1996 IEEE Petroleum and Chemical Industry Conference, Sept. 1996.
- [2] E. Persson, "Transient Effects in Application of PWM Inverters to Induction Motors," IEEE IAS Transactions, vol. 28. No. 5, Sept./Oct. 1992, P1095.
- [3] Hayt, W. H., 1989. *Engineering Electromagnetics*. New York: McGraw-Hill, Inc.
- [4] Takahashi, M. Termeyer, T. Lowery, and H. Tsai, "Motor Lead Length Issues for IGBT drives," 1995 IEEE Pulp and Paper Conference, pp. 21-27.
- [5] G. Skibinski, J. Erdman, and J. Pankau, "Assessing AC Motor Dielectric Withstand Capability to Reflected Voltage Stress using Corona Testers," IEEE IAS Conference Proceedings, 1996, pp. 694-702.
- [6] S. Van Haute, A. Malfait, R. Reekmans, and R. Belmans, "Losses, Audible Noise, and Overvoltage in Induction Motor Drives," IEEE PESC 1995, pp. 585-592.
- [7] G. Skibinski, D. Leggate, and R. J. Kerkman, "Cable Characteristics and Their Influence on Motor Over-Voltages," APEC Conference Proceedings 1997.
- [8] G.L. Skibinski and D. M. Divan, "Design Methodology & Modeling of Low Inductance Planar Bus Structures," EPE Conference 1993, Brighton, pp. 98-105.
- [9] L. Gubbala, A. von Jouanne, P. Enjeti, C. Singh, and H. Toliyat, "Voltage Distribution in the Windings of an AC Motor Subjected to High dv/dt PWM Voltages", IEEE PESC Conference Proceedings, 1995, pp. 579-585.
- [10] A. von Jouanne, and P. Enjeti, "Design Considerations for an Inverter Output Filter to Mitigate the Effects of Long Motor Leads in ASD Applications," APEC, 1996, pp. 579-585.
- [11] A. von Jouanne, P. Enjeti, and W. Gray, "The Effect of Long Motor Leads on PWM Inverter Fed AC Motor Drive Systems," IEEE APEC Conference Proceedings, 1995, pp. 592-597.
- [12] P. Van Paucke, R. Belmans, W. Geysen, and E. Ternier, "Overvoltages in Inverter Fed Induction Machines Using High Frequency Power Electronic Components," IEEE APEC Conference Proceeding 1994, pp. 536-541.
- [13] C. J. Melhorn and L. Tang, "Transient Effects of PWM ASDs on Standard Squirrel Cage Induction Motors," IEEE IAS Conference Proceedings 1995, pp. 2689-2695.
- [14] B. Kawkabani, J.J. Simond, and F. Kehtari, "Voltage Peaks of Low Voltage Motors Due to PWM Inverter Supply," EPE Conference Proceedings 1995, Sevilla, pp. 465-469.
- [15] Boris Mokrytzki, "Filters for Adjustable Frequency Drives," IEEE APEC Conference Proceedings, 1994, pp. 542-548.
- [16] R. J. Kerkman, D. Leggate, and G. Skibinski, "PWM Inverters and Their Influence on Motor Over-Voltages," APEC Conference Proceedings 1997.
- [17] G. Skibinski, "Apparatus Used with AC Motors for Eliminating Line Voltage Reflections," US Patent Pending.
- [18] A. von Jouanne, D. Rendusara, P. Enjeti, and W. Gray, "Filtering Techniques to Minimize the Effect of Long Motor Leads on PWM Inverter Fed AC Motor Drive Systems," IEEE IAS Conference Proceedings, 1995, pp. 37-44.
- [19] G. Skibinski, "Design Methodology of a Cable Terminator to Reduce Reflected Voltage on ac Motors." IEEE IAS Conference Proceedings 1996.